Peptide Sequence Effects Control the Single Pot Reduction, Nucleation, and Growth of Au Nanoparticles

Catherine J. Munro[1], Zak E. Hughes[2], Tiffany R. Walsh,[2] and Marc R. Knecht[1,*]

[1]Department of Chemistry, University of Miami, 1301 Memorial Drive, Coral Gables, Florida 33146, United States.
[2]Institute for Frontier Materials, Deakin University, Geelong, VIC 3216, Australia.

ABSTRACT: Peptides have demonstrated unique capabilities to fabricate inorganic nanomaterials of numerous compositions through non-covalent binding of the growing surface in solution. In this contribution, we demonstrate that these biomolecules can control all facets of Au nanoparticle fabrication, including Au^{3+} reduction, without the use of secondary reagents. In this regard using the AuBP1 peptide, the N-terminal tryptophan residue is responsible for driving Au^{3+} reduction to generate Au nanoparticles passivated by the oxidized peptide in solution, where localized residue context effects control the reducing strength of the biomolecule. The process was fully monitored by both time-resolved monitoring of the growth of the localized surface plasmon resonance and transmission electron microscopy. Nanoparticle growth occurs by a unique disaggregation of nanoparticle aggregates in solution. Computational modeling demonstrated that the oxidized residue of the peptide sequence does not impact the biomolecule's ability to bind the inorganic surface, as compared to the parent peptide, confirming that the biomolecule can be exploited for all steps in the nanoparticle fabrication process. Overall, these results expand the utility of peptides for the fabrication of inorganic nanomaterials, more strongly mimicking their use in nature via biomineralization processes. Furthermore, these capabilities enhance the simplicity of nanoparticle production and could find rapid use in the generation of complex multicomponent materials or nanoparticle assembly.

Introduction

Bio-inspired approaches for the controlled fabrication of nanostructures represent intriguing and potentially sustainable methods to access materials with enhanced properties for applications ranging from catalysis to biosensing. DNA,[1,2] viruses,[3,4] and peptides [5-9] have all been used in nanomaterial synthesis resulting in a range of particle size, shape, and functionality, indicating that the passivant can impact the structure/function relationship. A common synthetic approach employed for the preparation of noble metal nanoparticles mixes the biomolecules with the metal ions at selected stoichiometric ratios. Upon complexation, an exogenous reductant is added, driving metal ion reduction, leading to zerovalent nanoparticle nucleation and growth. As the inorganic structure grows in solution, the biomolecules bind to the material through a series of non-covalent interactions, impeding growth and controlling particle size.

While a variety of biomolecules have been used to generate inorganic nanomaterials, peptides are particularly promising due to their inherent molecular recognition capabilities that can be exploited to achieve compositionally selective binding. A significant number of peptide sequences with affinity to specific inorganic surfaces have been identified by biocombinatorial selection methods such as cell-surface and phage display.[5,10] From this, peptides with affinity for metals, metal oxides, and metal sulfides have been identified and used to investigate nanoparticle formation and structure/function relationships.[11-13] Sarikaya and coworkers isolated the AuBP1 sequence (WAGAKRLVLRRE), which has a high affinity for Au surfaces[14] and rivals the binding of alkane thiols on Au.[15] The peptide presents five anchor residues (W1, A4, R6, R10, and R11), which demonstrate persistent contact with the Au material.[14] In general, AuBP1 has been used under a variety of conditions to fabricate Au nanoparticles; however, the inherent sequence of the peptide, containing an important tryptophan anchor residue, suggests additional functionality not typically considered for peptides with materials specific binding affinity.

Previous studies of individual amino acids and short trimer peptides have suggested that tryptophan may possess the ability to reduce metal ions to their zerovalent form. From this residue, inorganic nanoparticles could be generated using the peptide alone without the need of an exogenous reductant. Such an effect would more closely mimic biomineralization approaches observed in biological systems and would enhance the sustainability of peptide-driven materials approaches. Tan *et al.* have shown that tyrosine and tryptophan free amino acids are the most promising to reduce Au^{3+} to Au^0.[16] Interdigitated peptides were used to enhance the binding affinity and engender the biomolecules with the ability to reduce Au^{3+} ions; however, the selectivity of the peptide for the Au surface and the effects of the oxidized peptide on inorganic affinity remain unexplored. What is clear, however, is that the reduction strength of the interdigitated peptide is not simply the sum of the activity of the individual residues within the sequence. More complex peptides such as the AuBP1 could display significantly altered reduction and material binding capabilities compared to the physical mixtures of the independent amino acids.

Further work by Si and Mandal exploited synthetic trimer peptides with a tryptophan at the C-terminus for the fabrication of Au and Ag nanoparticles under basic conditions.[17] Here it was again suggested that the tryptophan residue was responsible for particle reduction, potentially by electron transfer where tryptophan is oxidized to the tryptophyl radical before generating a kynurenine residue, as well as other dimerized products. While this work suggests that tryptophan possesses the ability to reduce Au^{3+}, a complete understanding of how this process occurs remains poorly understood. This includes the effects of tryptophan oxidation on peptide affinity, how the oxidized peptide interacts with the Au surface, how the peptide sequence effects Au^{3+} reduction, and how this unique bio-driven reduction process alters nanoparticle structures. It is likely that this process is substantially different from standard nanoparticle fabrication approaches, thus an in depth study focused on material growth and biomolecular binding events is required.

In this contribution, we have exploited the AuBP1 peptide to examine the effects of biomolecule-driven reduction, nucleation, growth, and passivation of Au nanoparticles in a single pot. In this regard, the peptide simultaneously acts as both the *in situ* reductant and surface passivant, which has been probed both experimentally and computationally. The peptide-driven Au^{3+} reduction event was monitored by UV-vis analysis of the localized surface plasmon resonance (LSPR) band of the growing Au nanoparticles. The nanoparticles generated in this approach were fully characterized using transmission electron microscopy (TEM), including an examination of peptide concentration effects as well as the growth of the particles throughout the reduction reaction. Additionally, metadynamics simulations were used to predict and compare the binding free energies of both the kynurenine and tryptophan amino acids at the aqueous Au interface, and Replica Exchange with Solute Tempering (REST) molecular dynamics (MD) simulations were used to predict the likely structures of AuBP1 in the tryptophan-oxidized state when adsorbed at the interface. Interestingly, the results suggest that under acidic conditions the tryptophan residues are oxidized to drive Au nanoparticle fabrication where kynurenine may not be the sole oxidized product. Furthermore, the positioning of the tryptophan residue played a significant role in the reduction rate; however, it did not substantially change the final structure of the inorganic materials. Such effects are important for use in the single pot generation of Au nanoparticles via biomimetic approaches, which could be exploited for the fabrication of intricate structures rivaling the complexity and diversity of biology for application in optics, sensing, catalysis, materials assembly, etc.

Experimental section

Materials. $HAuCl_4$ was purchased from Acros Organics while trifluoroacetic acid (TFA) and tri-isopropyl silane (TIS) were purchased form Alfa Aesar. Acetonitrile, methanol, and *N*,*N*-dimethylformamide (DMF) were purchased form BDH, whereas all FMOC-protected amino acids and derivatives, Wang resins, and coupling reagents were acquired from Advanced Chemtech. L-Alanine, L-Lysine, L-Tryptophan, and L-Arginine came from Sigma Aldrich. The remaining amino acids, L-Glycine and L-Leucine, were purchased from TCI. All reagents were used as received and ultrapure water (18.2 MΩ·cm) was employed in all experiments.

Peptide Synthesis. Solid phase peptide synthesis was used following standard protocols on a TETRAS peptide synthesizer (Creosalus).[18] Peptides were cleaved from the Wang resins using a cocktail of TIS/H_2O/TFA (25 μL: 25 μL: 950 μL) and purified using reverse-phase high performance liquid chromatography (HPLC) (Waters). The purified peptides were confirmed using matrix-assisted laser desorption/ionization time-of-flight (MALDI-TOF) mass spectrometry.[18]

Peptide-Induced Reduction Reaction. Each peptide-driven reduction reaction was processed at a constant Au^{3+} concentration, while the peptide concentration varied such that the peptide:Au^{3+} ratio ranged from 1-5. A description of the reaction for a ratio of 1 is described below; however, changes in the volume of peptide solution and water added were used to change the ratio and maintain a constant reaction volume. To a well in a clear 96-well plate, 20.0 μL of an aqueous 1.0 mM peptide solution was diluted in 160.0 μL of water. To this mixture, 20.0 μL of 1.0 mM $HAuCl_4$ in water was added and the mixture was slightly agitated. The well plate was subsequently inserted into the plate reader (Synergy|Mx) to monitor the UV-vis absorbance of the material for 1600 min to ensure that the reaction reached completion.

Characterization. TEM analysis was performed using a JEOL JEM-2010 microscope operating at 80 kV. The samples were prepared by drop-casting 5 μL of the nanoparticle solution on to a carbon-coated 200 mesh Cu grid (EM Sciences) and allowed to dry overnight. Sizing of the generated materials was performed on all grids over at least ten images for each grid, including at least 300 particles at their widest sections.

Modeling. Two types of molecular simulations were utilized. Both cases used the polarizable force-field for the Au surface, GolP-CHARMM.[19] First, well-tempered multiple-walker metadynamics simulations[20-22] describing the adsorption of the Kyn residue, blocked at both the N- and C-termini, was performed at the aqueous Au(111) interface using the PLUMED plugin.[23] Second, a

REST simulation[24,25] was performed on the AuBP1 kyn sequence adsorbed at the aqueous Au(111) interface. Based on previously-published analyses, this surface is thought to be the dominant facet at the aqueous interface of polycrystalline Au.[26] Additional information, including full details of the metadynamics simulations and REST-MD simulations, and their analyses, can be found in the Supporting Information: Computational Details. Recently, the capabilities of the GolP-CHARMM forcefield have demonstrated near-reproduction of the experimentally-determined binding free energy of the AuBP1 peptide at the aqueous Au interface.[26]

Results and Discussion

Peptides have been extensively used to fabricate noble metal nanoparticles, especially of Au;[1,27] however, they require the use of an exogenous reductant to drive reduction of Au^{3+} ions to Au^0. It would be ideal for a peptide to control all steps of the fabrication process, including the metal ion reduction step. Previous studies have suggested that tryptophan could achieve this capability,[17,28-30] but it remains unclear how such a residue, which is known to have significantly strong interactions with the metallic surface,[14,31] can control this process when integrated into a peptide sequence. Furthermore, how peptide oxidation affects Au binding compared to the parent biomolecule remains unstudied. For instance, context effects, defined as the effects of local residues in proximity to tryptophan, could alter the reducing power of the residue. As such, an in depth study to elucidate these capabilities is required where both experimental and computational approaches must be used. This includes a fundamental understanding of the binding event at the growing nanoparticle surface of the oxidized biomolecule, as well as identification of the particle growth mechanism in solution that is likely to be different than standard monolayer protected Au clusters using alkanethiols. To study this effect, complementary experimental and computational approaches were exploited using the AuBP1 peptide, which was isolated with Au affinity and possesses an N-terminal Trp residue. Furthermore, this sequence has been extensively used for Au nanoparticle fabrication.[31,32]

The ability of the AuBP1 peptide to reduce Au^{3+} ions was initially studied using UV-vis spectroscopy (Figure 1a). In this study, the Au^{3+} ions are co-mixed with the peptides in water at a peptide:Au^{3+} ratio of 3, from which the solution color gradually changed from faint yellow to vibrant pink, indicative of Au nanoparticle formation. During this process, the growth of an LSPR band around 540 nm was evident over a reaction time of 1600 min. The UV-vis of the system shows an induction period followed by a surprising blue shift from 550 nm to the final position at 520 nm. Figure 1b monitors the growth of the LSPR at 540 nm over time at selected peptide:Au^{3+} ratios ranging from 1-5. In these studies, the peptide concentration increased while the Au^{3+} concentration in the reaction remained constant. In this analysis, the rate of plasmon growth clearly increases as the concentration of the peptide also increases. From these data, the pseudo first-order rate constants (k) were calculated by standard approaches (Figure 1c).[33,34] Briefly, the natural log of the absorbance at 540 nm, divided by the initial absorbance at this wavelength, was plotted as a function of time. The data was subsequently fit with a linear best fit line, from which the slope of this line represents the pseudo first order rate constant. Interestingly, when the AuBP1:Au^{3+} ratio was set at 1, a k value of $(1.87 \pm 0.06) \times 10^{-3}$ min^{-1} was determined, which increased in magnitude as the amount of peptide in the reaction increased to a ratio of 5, resulting in a rate constant of (6.17 ± 0.49)

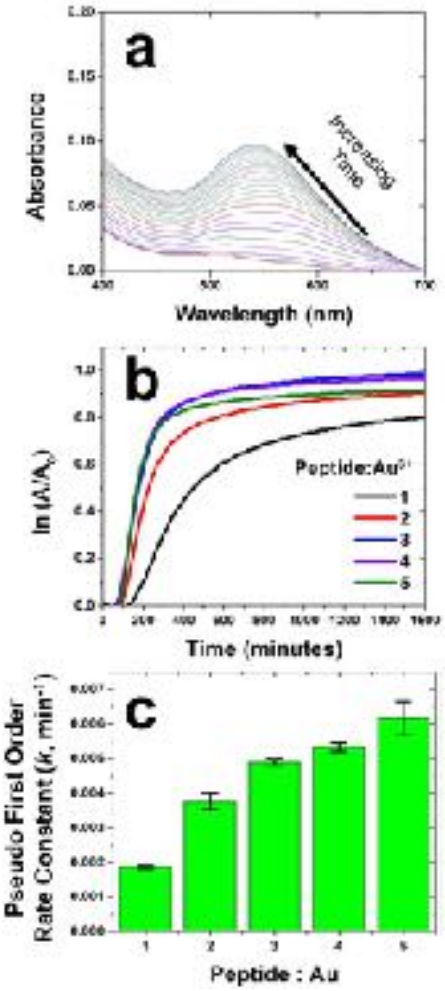

Figure 1. (a) UV-vis analysis of Au^{3+} reduction in the presence of AuBP1 at a peptide:Au^{3+} ratio of 3. (b) Pseudo-first order kinetic analysis of the reduction of Au^{3+} in the presence of AuBP1 at peptide:Au^{3+} ratios of 1 to 5. (c) Calculated k values for the reduction of Au^{3+} in the presence of AuBP1 at peptide:Au^{3+} ratios of 1 to 5.

$\times 10^{-3}$ min^{-1}. Such results strongly indicate that the peptide itself is capable of driving the chemical reduction process where no bulk precipitate was noted even after 1600 min of reaction. The lack of precipitation suggests that the peptide that is oxidized during the metal ion reduction process retains sufficient affinity for the Au surface to stabilize the growing nanoparticles dispersed in solution.

After completion of the peptide-driven reduction process, the Au particles generated at each AuBP1:Au^{3+} ratio were imaged using TEM (Figure 2). In general, spheroidal-shaped metallic materials were fabricated, which were stabilized by the peptide in the reaction mixture. Note that when the reaction was processed in the absence of peptide, no Au^{3+} reduction was observed, thus no TEM analysis of the peptide-free control could be studied. When the materials prepared at a peptide:Au^{3+} ratio of 1 were analyzed (Figure 2a), Au nanoparticles with an average diameter of 20.2 ± 9.2 nm were observed. As the peptide concentration increased in the reaction (Figures 2b-d), a minor shift towards smaller material sizes was noted where an average diameter of 17.0 ± 5.4 nm was observed for the materials prepared at a ratio of 5 (Figure 2e). While the average size showed only a minor change, the distribution in the nanoparticle sizes observed in each sample notably diminished when higher concentrations of peptides were used in the reaction. Such a distribution effect was to be anticipated as additional peptide was present in the reaction mixture to ensure efficient passivation of the growing Au nanoparticle surface at higher peptide:Au^{3+} ratios.

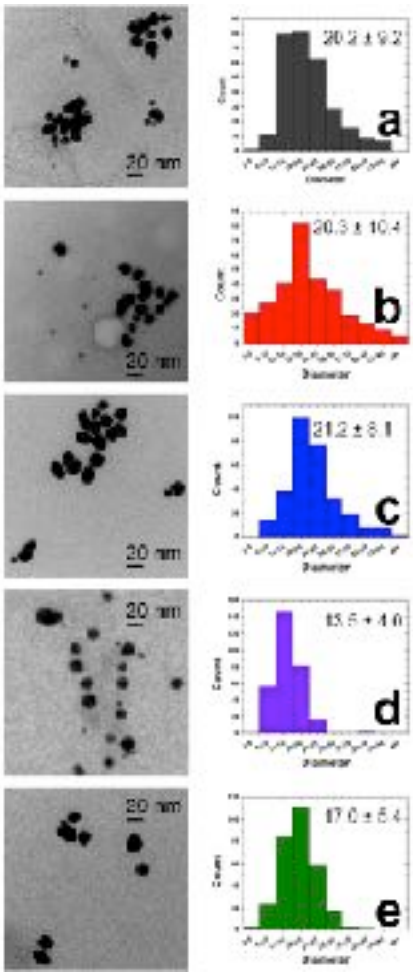

Figure 2. TEM images (left) and particle size distribution histograms (right) of AuBP1 driven Au^{3+} reduction after 1000 min at peptide:Au^{3+} ratios of (a) 1, (b) 2, (c) 3, (d) 4, and (e) 5.

While it is evident that the AuBP1 peptide is driving the reduction of Au^{3+} ions in solution, the mechanism of such a process remains unclear. Interestingly, while Au nanoparticles of ~10-20 nm are generated, the UV-vis studies suggest a unique process is occurring to result in these structures. Here, a clear blue shift in the LSPR band of the growing materials is evident from 550 nm to 520 nm throughout the reaction. This would suggest that changes in particle size from larger to smaller are observed during the Au nanoparticle formation process. Typically Au nanoparticles nucleate at individual sites and then grow via Au atom adsorption onto the nuclei.[35] Once the particle surface is passivated with the ligand in solution, the reaction is quenched to maintain the particle size, thus the particles grow from the atomic scale to the larger nanoscale regime. In this approach, a red shifting LSPR peak would be anticipated as the materials grow from smaller to larger.

To monitor the growth mechanism of the peptide-based reduction process, TEM imaging of the materials throughout the reaction at a peptide:Au^{3+} ratio of 3 was processed (Figure 3). For this, an aliquot of the reaction was removed from the solution, rapidly added to TEM grid sur face, and then allowed to dry in a desiccator. Once dried, the materials deposited on the grid surface were imaged and analyzed for changes in particle dimensions as a function of reaction progression. Figure 3a presents the image of the materials after 60 min of reduction, while Figure S4 in the Supporting Information provides an additional image at lower magnification. In this sample, large, dendritic-like inorganic materials were observed, where it appeared as if individual Au nanoparticles were arranged to generate the large structure. Sizing analysis of the materials demonstrated that the average width of the global structure was 80.2 ± 37.2 nm. This analysis was completed across the entire width of the structure from the largest dimension. Unfortunately, measurements of the individual components of the aggregated structure could not be assessed due to the significant overlap between the different particle components.

When the reaction materials generated after 248 min of reduction were studied, a clear shift in material morphology was noted (Figure 3b). For this time point, a polydisperse set of materials was observed, where both individual Au nanoparticles and nanoparticle aggregates were noted in this sample. The average material sizes were calculated, where a shift to a smaller dimension of 29.4 ± 10.3 nm was seen. Note that this measurement incorporates both material populations into a single histogram for the individual particles and the width of nanoparticle aggregates, which gives rise to the significantly broad particle **Figure 3.** TEM images (left) and particle size distribution histograms (right) of AuBP1-driven Au^{3+} reduction at a peptide:Au^{3+} ratio of 3 after (a) 60, (b) 248, (c) 436, (d) 624, (e) 812, and (f) 1000 min of reduction.

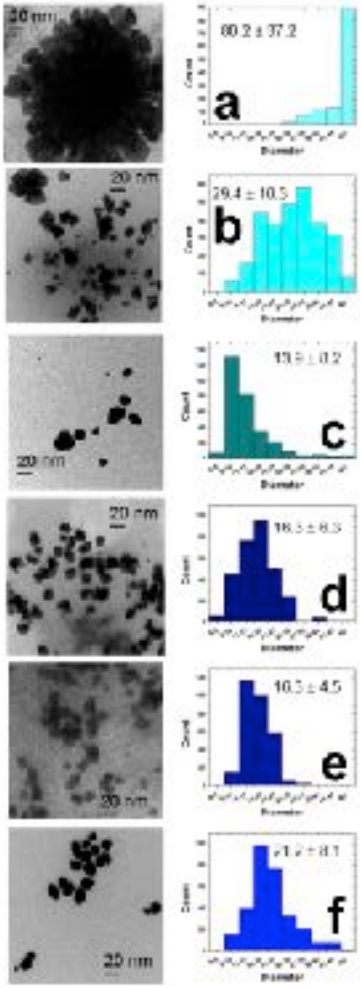

distribution analysis. Due to difficulties in distinguishing between individual particles and smaller particle aggregates, bifurcating the measurement into two populations was not possible. After 436 min of reduction (Figure 3c), analysis of the materials demonstrated only individual Au nanoparticles on the TEM grid, where no nanoparticle aggregates were observed. For these materials, a particle diameter of 13.9 ± 8.2 nm was noted, where the average particle size remained roughly constant after longer times of reduction (Figure 3d-f). From this time-based analysis, it is evident that large, Au nanoparticle aggregated structures are rapidly formed by peptide-driven reduction and eventually disaggregate throughout the reaction process. This gives rise to the observed blue shifts in the UV-vis spectrum of the material LSPR. Such a disaggregation process is unique compared to standard nanoparticle growth mechanisms.

While a distinctive Au nanoparticle growth mechanism appears to be evident, the basis of the reductant capability of the AuBP1 remains poorly understood. Previous studies have indicated that individual amino acids can drive the reduction of metal ions to the zerovalent state;[10,17,29,36] however, varying degrees of reduction strength are possible. In general, tryptophan has been demonstrated to have significant reducing capabilities to generate Au^0 from Au^{3+} ions. [10,17,29,36] In basic media, this process occurs through deprotonation of the tryptophan by the base, where the amino acid is then oxidized to generate kynurenine as well as other oxidative products; however, the effects of the amino acid sequence and composition of peptide remains poorly understood. Peptide sequence effects are known to alter the global properties of the biomolecules,[16] thus they are likely to shift the reducing capabilities of the tryptophan residue.

To probe peptide-based metal ion reducing capabilities, two control peptides with known affinity for Au were studied for Au^{3+} reduction: AuBP2 (WALRRSIRRQSY) and Pd4 (TSNAVHPTLRHL).[14] These two sequences were selected as the AuBP2 peptide possesses a tryptophan residue, while the Pd4 does not, thus serving as ideal positive and negative controls of tryptophan-driven Au^{3+} reduction. Using these two peptides, anticipated degrees of Au^{3+} reduction capabilities were observed, as shown in Figure 4. The *k* values of the AuBP1 driven system are shown for comparison (Figure 4a). Here, the AuBP2 sequence was able to drive the reduction process at the selected peptide:Au^{3+} ratios with rate constants ranging from (1.97 ± 0.06) × 10^{-3} min^{-1} to (5.77 ± 0.12) × 10^{-3} min^{-1} at ratios of 1 and 5, respectively. Such values are similar to those observed with the initially studied AuBP1 peptide. Note that the both the AuBP1 and AuBP2 peptides have N-terminal tryptophan residues followed by an alanine. As such, the local environment for the tryptophan is similar. TEM analysis (Figure 4b) of the Au nanoparticles generated via AuBP2 reduction at a peptide:Au^{3+} ratio of 3 after 1000 min demonstrated polydisperse particles of sizes comparable to those generated using the AuBP1 (6.3 ± 4.1 nm) When using the Pd4 peptide as the reductant, no Au nanoparticle formation was observed due to a lack of LSPR formation over the time frame of the reaction, consistent with the lack of reduction capabilities, regardless of the Pd4:Au^{3+} ratio employed. This strongly supports the

effect of the tryptophan being responsible for the metal ion reduction process.

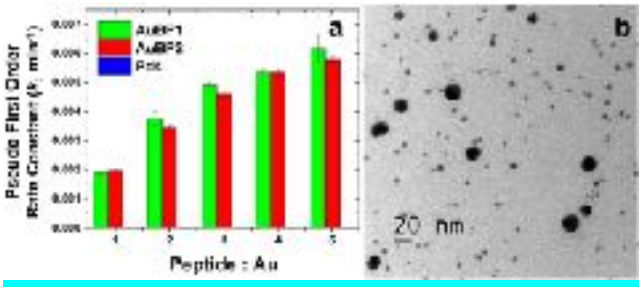

Figure 4. Au^{3+} reduction capability comparison of the AuBP2 and Pd4 peptides to AuBP1. Part (a) compares the first order rate constants as a function of the peptide:Au^{3+} ratio, while part (b) presents a TEM image of Au nanoparticles made by AuBP2 after 1000 min of reduction using an AuBP2:Au^{3+} ratio of 3.

While the positive (AuBP2) and negative (Pd4) controls confirmed the activity of the tryptophan residue for Au^{3+} reduction, they did not probe the effects of the residue context within the peptide sequence. To probe these effects, a series of AuBP1 peptides with modified sequences or individual amino acids were probed (Figure 5). For instance, when physical mixtures of the individual amino acids of the AuBP1 peptide were dissolved with Au^{3+} ions at the concentrations that they would be

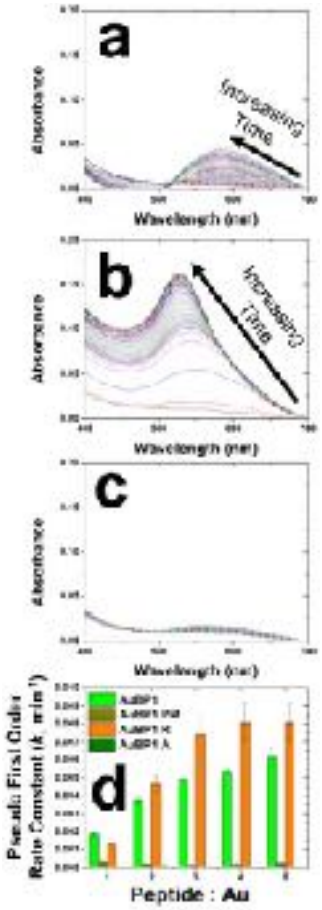

at using the peptides, negligible metal ion reduction was noted (indicated

Figure 5. (a) UV-vis analysis of Au^{3+} reduction in the presence of the physical mixture of individual amino acids of the AuBP1 at a peptide:Au^{3+} ratio of 3. (b) UV-vis analysis of Au^{3+} reduction in the presence AuBP1 R at a peptide:Au^{3+} ratio of 3. (c) UV-vis analysis of Au^{3+} reduction in the presence AuBP1 A at a peptide:Au^{3+} ratio of 3. (d) Comparison of the calculated k values for the reduction of Au^{3+} in the presence of AuBP1, AuBP1 PM, AuBP1 R, and AuBP1 A at peptide:Au^{3+} ratios of 1 to 5.

as AuBP1 PM in Figure 5a and d). From this, the maximum rate constant of Au^{3+} reduction was $(0.3 \pm 0.2) \times 10^{-3}$ min^{-1}, which is six times lower than values obtained for the AuBP1 peptide. This indicates that integrating the tryptophan residue into a peptide sequence is critically important in controlling the overall reduction capabilities. Furthermore, a new peptide sequence was generated where the tryptophan residue of the AuBP1 was swapped for an alanine (termed AuBP1 A – Figure 5c). This modification resulted in complete loss of peptide-driven Au^{3+} reduction, further confirming the reactivity of the tryptophan. Finally, a second modified AuBP1 peptide was synthesized where the residue order was randomized to generate a new sequence (termed AuBP1 R – VRGERLKAWLAR; Figure 5b). Note that the tryptophan residue is no longer at one of the peptide termini, but buried within the sequence. When using this peptide to reduce Au^{3+}, a substantial increase in reactivity was observed, where the k values at the selected ratios were generally greater than those for the parent AuBP1 peptide. For instance, at a peptide:Au^{3+} ratio of 5, the AuBP1 driven reduction process demonstrated a k value of $(6.17 \pm 0.49) \times 10^{-3}$ min^{-1}; however, using the AuBP1 R system, a rate constant of $(8.1 \pm 1.08) \times 10^{-3}$ min^{-1} was calculated.

Based upon these results, it is clear that the tryptophan residue is responsible for the reduction of Au^{3+} ions, while the entire peptide mediates the growth, passivation, and stabilization of Au nanoparticles in solution. Furthermore, the reducing capabilities appear to be context specific, where the neighboring residues of the tryptophan, as well as potentially the entire peptide sequence, plays a role in modulating the reducing strength. In the mechanism proposed by Si and Mandal, under basic conditions, tryptophan is oxidized to the tryptophyl radical in the presence of Au^{3+} ions before it reacts to form ditryptophan, *N*-formyl-kynurenine, kynurenine, and other cross-linked products. [17,30] Note that the present system is being studied under acidic conditions (pH 3.49). To probe the effects of an oxidized product on the observed peptide reduction and binding process, kynurenine, a significant oxidation product of tryptophan, was substituted into the AuBP1 peptide to replace tryptophan. If kynurenine was the final product,

then the new oxidized N-terminus could significantly alter the binding affinity of the oxidized peptide to the Au surface, as well as the reduction capability of the peptide.

AuBP1 kyn (kynAGAKRLVLRRE) was synthesized, substituting tryptophan with the oxidation product kynurenine, to understand the effects of the oxidized biomolecule on the reduction of Au^{3+} and its binding to the aqueous Au^0 surface. To compare the binding affinity of AuBP1 to AuBP1 kyn, Quartz Crystal Microbalance (QCM) studies were performed on Au sensors. In this analysis, increasing concentrations of AuBP1 kyn were flowed over Au sensors and the frequency change of the sensors were measured as the peptide adsorbed to the metallic surface. This adsorption was modeled using a Langmuir fit to extrapolate ΔG for the binding of AuBP1 kyn using previously described approaches.[14] The ΔG determined for AuBP1 kyn binding was -37.8 ± 5.2 kJ/mol, which is nearly identical for the value previously quantitated for AuBP1 on Au (-37.6 ± 0.9 kJ/mol).[14] This indicates that the binding affinity of the oxidized biomolecule shows no significant difference compared to the binding affinity of the initial peptide.

Computational modeling further corroborated this finding. First, metadynamics MD simulations were used to predict the binding free energy of independent kynurenine (*i.e.* in amino acid form) at the aqueous Au interface. By integrating the change in free energy (see Computational Details in the Supporting Information) as a function of distance from the surface (see Figure S15 in the Supporting Information for both Trp and Kyn), the free energy of adsorption was obtained and calculated to be -20.3 ± 0.8 kJ mol^{-1} for Kyn, while the corresponding value for Trp was -19.7 ± 2.4 kJ mol^{-1}. These data indicate that the adsorption free energy for both residues can be considered equivalent (within error). Thus Kyn, like Trp can serve as a very strong anchor residue at the aqueous Au interface.

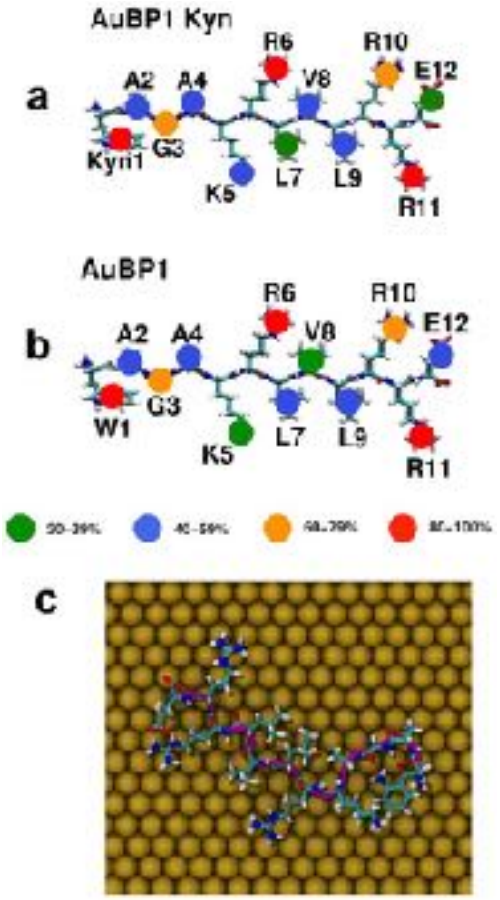

Figure 6. (a) Summary of the contact residue data for the AuBP1 kyn sequence adsorbed at the Au aqueous interface. For each residue, we give the percentage of the entire REST-MD reference trajectory (%) that each residue is determined to be in contact with the surface. (b) Corresponding contact data for the parent AuBP1 sequence[31], are shown for comparison. (c) Representative structure (plan view) of AuBP1 kyn adsorbed at the aqueous Au (111) interface. The Au(111) surface is a widely accepted model for the Au substrate (see methods). Water molecules not shown for clarity.

To investigate how the peptide environment affected the surface adsorption of the Kyn residue, REST-MD simulations were performed on the AuBP1 kyn sequence adsorbed at the aqueous Au interface. From these simulations, the degree of surface contact was calculated for each residue. These findings were compared to the findings for the parent AuBP1 peptide,[14] as summarized in Figure 6a (see Table S1 in the Supporting Information for numerical values). Overall, the number and location of key anchor residues in AuBP1 appear to have been preserved in AuBP1 kyn. This means the general binding mode of AuBP1 kyn is predicted to be very similar with that of AuBP1, where a representative adsorbed structure of AuBP1 kyn is illustrated in Figure 6b.

Once the binding analysis of the AuBP1 kyn peptide was more fully understood, its ability to reduce Au^{3+} ions was examined (Figure 7a). Using identical methods as

Figure 7. (a) UV-vis analysis of Au^{3+} reduction in the presence of AuBP1 kyn at a peptide:Au^{3+} ratio of 3. (b) TEM analysis of particles made with AuBP1 kyn at a peptide:Au^{3+} ratio of 3. (c) pseudo-first order kinetic analysis of the reduction of Au^{3+} in the presence of AuBP1 kyn at peptide: Au^{3+} ratios of 1-5. (d) A comparative bar chart of the calculated k values for the reduction of Au^{3+} in the presence of AuBP1 and AuBP1 kyn.

employed with the parent AuBP1, increasing amounts of AuBP1 kyn were exposed to a constant amount of Au^{3+} where substantially diminished k values were noted for the reduction reaction. As shown in Figure 7c and d, the reduction rate of Au^{3+} to Au^0 for the kynurenine-baring

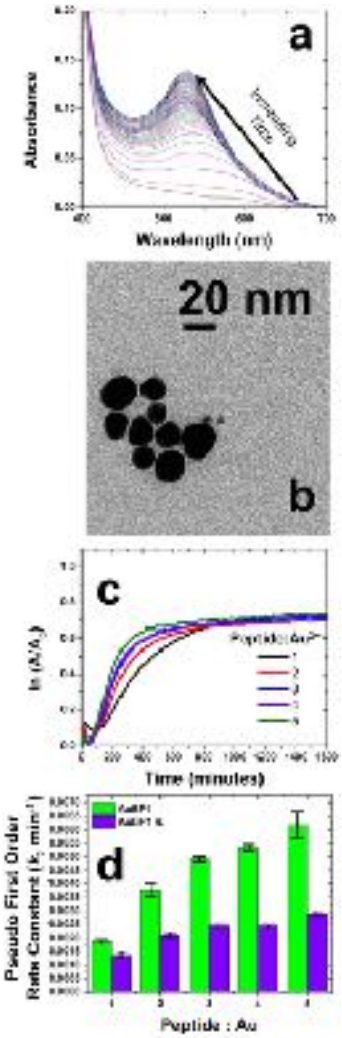

peptide at a peptide:Au^{3+} ratio of 1 was (1.37 ± 0.11) × 10^{-3} min^{-1}, which was reduced compared to the AuBP1 under the same conditions. Note that the pH of the two system were very similar: 3.49 for AuBP1 and 3.65 for AuBP1 kyn. While greater *k* values were noted for the AuBP1 parent system as the peptide concentration increased, only minor *k* value changes were noted when the AuBP1 kyn peptide concentration was increased. As such, the rate constants for the kynurenine-containing molecules were substantially lower as compared to the parent. Interestingly, TEM analysis (Figure 7b) indicated that the particles generated using the AuBP1 kyn peptide were smaller with an average size of 8.5 ± 4.1 nm using a peptide:Au^{3+} ratio of 5.

These results using the AuBP1 kyn peptide demonstrate that the oxidation of the peptide presents minimal changes on the affinity of the biomolecule to the target surface; however, in the presence of AuBP1 kyn, continued oxidation of the kyn residue persists for Au^{3+} reduction. This suggests that while kyn may be an intermediate product during AuBP1 driven Au^{3+} reduction via tryptophan oxidation, this may not be the final product under acidic conditions. Previous work demonstrated reactivity under basic conditions, where the current acidic conditions are likely to alter reactivity pathways where additional solution conditions may alter/affect the overall reactivity. Due to the small amount of peptide in the reaction mixture, mass spec analysis of the biomolecule after Au nanoparticle formation could not be processed; however, additional studies are presently underway to further understand this unique bio-based reduction capability.

Conclusions

In conclusion, these results demonstrate that biomolecules are highly unique with the ability to fabricate Au nanoparticles from Au^{3+} reduction to surface passivation and stabilization without the use of additional reagents. Such capabilities are important for sustainable nanoparticle production and could be important for specific applications where deposition of nanoparticles at specific locations is required. The reduction activity was determined to arise from a Trp residue within the peptide sequence, where the reactivity is sensitive to the local environment surrounding the residue. This effect was confirmed using synthetic mutation studies, as well as positive and negative control sequences. Interestingly, nanoparticle growth by this mechanism follows a unique disaggregation process from large material aggregates, as observed by TEM and a blue shifting LSPR. Furthermore, as confirmed by computational modeling, oxidation of the Trp residue in the biomolecule imparts negligible changes on the peptide Au affinity or binding pattern, thus indicating that the Au^{3+} reduction process does not diminish the ligand's ability to passivate the metallic surface. Overall, such multifunctional capabilities from a single peptide ligand are highly attractive and simplify material fabrication schemes. Additional effects of solution conditions and the overall peptide sequence are likely to further modify the Au nanoparticle reduction process, all of which are currently under study in our laboratories.

ASSOCIATED CONTENT

Supporting Information

Additional UV-vis time traces, TEM images, and kinetic plots for the peptide mutants and control reactions, additional computational details, calculated free energy profiles and structures, and numerical values of AuBP1 kyn surface contact. The Supporting Information is available free of charge on the ACS Publications website.

AUTHOR INFORMATION

Corresponding Author

*MRK: Phone: (305) 284-9351. E-mail: knecht@miami.edu.

ACKNOWLEDGMENT

This material is based upon work supported by the Air Force Office of Scientific Research, grant number FA9550-12-1-0226. We gratefully acknowledge the Victorian Life Science Computation Facility (VLSCI) for allocation of

computational resources, and TRW thanks **veski** for an Innovation Fellowship.

REFERENCES

1. Han, M. S.; Lytton-Jean, A.K.R.; Oh, B.-K.; Heo, J.; Mirkin, C. A. Colorimetric Screening of DNA-Binding Molecules with Gold Nanoparticle Probes. *Angew. Chem., Int. Ed.* **2006**, *45*, 1807-1810.

2. Lee, J.-S.; Lytton-Jean, A. K. R.; Hurst, S. J.; Mirkin, C. A. Silver Nanoparticle−Oligonucleotide Conjugates Based on DNA with Triple Cyclic Disulfide Moieties. *Nano Lett.* **2007**, *7*, 2112-2115.

3. Lee, S.-W.; Mao, C.; Flynn, C. E.; Belcher, A. M. Ordering of Quantum Dots Using Genetically Engineered Viruses. *Science* **2002**, *296*, 892-895.

4. Lee, Y. J.; Yi, H.; Kim, W.-J.; Kang, K.; Yun, D. S.; Strano, M. S.; Ceder, G.; Belcher, A. M. Fabricating Genetically Engineered High-Power Lithium-Ion Batteries Using Multiple Virus Genes. *Science* **2009**, *324*, 1051-1055.

5. Wei, Z.; Maeda, Y.; Kanetsuki, Y.; Shi, M.; Matsui, H. Screening of Oligopeptides That Recognize Inorganic Crystalline Facets of Metal Nanoparticles. *Isr. J. Chem.* **2015**, *55*, 749-755.

6. Bedford, N. M.; Ramezani-Dakhel, H.; Slocik, J. M.; Briggs, B. D.; Ren, Y.; Frenkel, A. I.; Petkov, V.; Heinz, H.; Naik, R. R.; Knecht, M. R. Elucidation of Peptide-Directed Palladium Surface Structure for Biologically Tunable Nanocatalysts. *ACS Nano* **2015**, *9*, 5082-5092.

7. Briggs, B. D.; Li, Y.; Swihart, M. T.; Knecht, M. R. Reductant and Sequence Effects on the Morphology and Catalytic Activity of Peptide-Capped Au Nanoparticles. *ACS Appl. Mater. Interfaces* **2015**, *7*, 8843-8851.

8. Coppage, R.; Slocik, J. M.; Ramezani-Dakhel, H.; Bedford, N. M.; Heinz, H.; Naik, R. R.; Knecht, M. R. Exploiting Localized Surface Binding Effects to Enhance the Catalytic Reactivity of Peptide-Capped Nanoparticles. *J. Am. Chem. Soc.* **2013**, *135*, 11048-11054.

9. Surujpaul, P. P.; Gutiérrez-Wing, C.; Ocampo-García, B.; de M. Ramírez, F.; Arteaga de Murphy, C.; Pedraza-López, M.; Camacho-López, M. A.; Ferro-Flores, G. Gold Nanoparticles Conjugated to [Tyr3]Octreotide Peptide. *Biophys. Chem.* **2008**, *138*, 83-90.

10. Sarikaya, M.; Tamerler, C.; Jen, A. K. Y.; Schulten, K.; Baneyx, F. Molecular Biomimetics: Nanotechnology through Biology. *Nat. Mater.* **2003**, *2*, 577-585.

11. Porta, F.; Speranza, G.; Krpetić, Ž.; Dal Santo, V.; Francescato, P.; Scarì, G. Gold Nanoparticles Capped by Peptides. *Mater. Sci. Eng., B* **2007**, *140*, 187-194.

12. Wang, Z.; Lévy, R.; Fernig, D. G.; Brust, M. The Peptide Route to Multifunctional Gold Nanoparticles. *Bioconjugate Chem.* **2005**, *16*, 497-500.

13. Naik, R. R.; Stringer, S. J.; Agarwal, G.; Jones, S. E.; Stone, M. O. Biomimetic Synthesis and Patterning of Silver Nanoparticles. *Nat. Mater.* **2002**, *1*, 169-172.

14. Tang, Z.; Palafox-Hernandez, J. P.; Law, W.-C.; E. Hughes, Z.; Swihart, M. T.; Prasad, P. N.; Knecht, M. R.; Walsh, T. R. Biomolecular Recognition Principles for Bionanocombinatorics: An Integrated Approach to Elucidate Enthalpic and Entropic Factors. *ACS Nano* **2013**, *7*, 9632-9646.

15. Tamerler, C.; Oren, E. E.; Duman, M.; Venkatasubramanian, E.; Sarikaya, M. Adsorption Kinetics of an Engineered Gold Binding Peptide by Surface Plasmon Resonance Spectroscopy and a Quartz Crystal Microbalance. *Langmuir* **2006**, *22*, 7712-7718.

16. Tan, Y. N.; Lee, J. Y.; Wang, D. I. C. Uncovering the Design Rules for Peptide Synthesis of Metal Nanoparticles. *J. Am. Chem. Soc.* **2010**, *132*, 5677-5686.

17. Si, S.; Mandal, T. K. Tryptophan-Based Peptides to Synthesize Gold and Silver Nanoparticles: A Mechanistic and Kinetic Study. *Eur. J. Chem.* **2007**, *13*, 3160-3168.

18. Chan, W. C.; White, P. D. Fmoc Solid Phase Peptide Synthesis: A Practical Approach, 2000.

19. Wright, L. B.; Rodger, P. M.; Corni, S.; Walsh, T. R. GolpCharmm: First-Principles Based Force Fields for the Interaction of Proteins with Au(111) and Au(100). *J. Chem. Theory Comput.* **2013**, *9*, 1616-1630.

20. Laio, A.; Parrinello, M. Escaping Free-Energy Minima. *Proc. Nat'l. Acad. Sci.* **2002**, *99*, 12562-12566.

21. Barducci, A. B., Giovanni; Parrinello, Michele. Well-Tempered Metadynamics: A Smoothly Converging and Tunable Free-Energy Method. *Phys. Rev. Lett.* **2008**, *100*, 020603.

22. Raiteri, P.; Laio, A.; Gervasio, F. L.; Micheletti, C.; Parrinello, M. Efficient Reconstruction of Complex Free Energy Landscapes by Multiple Walkers Metadynamics. *J. Phys. Chem. B* **2006**, *110*, 3533-3539.

23. Tribello, G. A.; Bonomi, M.; Branduardi, D.; Camilloni, C.; Bussi, G. Plumed 2: New Feathers for an Old Bird. *Comput. Phys. Commun.* **2014**, *185*, 604-613.

24. Wright, L. B.; Walsh, T. R. Efficient Conformational Sampling of Peptides Adsorbed onto Inorganic Surfaces: Insights from a Quartz Binding Peptide. *Phys. Chem. Chem. Phys.* **2013**, *15*, 4715-4726.

25. Terakawa, T.; Kameda, T.; Takada, S. On Easy Implementation of a Variant of the Replica Exchange with Solute Tempering in Gromacs. *J. Comput. Chem.* **2011**, *32*, 1228-1234.

26. Wright, L. B.; Palafox-Hernandez, J. P.; Rodger, P. M.; Corni, S.; Walsh, T. R. Facet Selectivity in Gold Binding Peptides: Exploiting Interfacial Water Structure. *Chem. Sci.* **2015**, *6*, 5204-5214.

27. Grzelczak, M.; Perez-Juste, J.; Mulvaney, P.; Liz-Marzan, L. M. Shape Control in Gold Nanoparticle Synthesis. *Chem. Soc. Rev.* **2008**, *37*, 1783-1791.

28. Hussain, S.; Pang, Y. Surface Geometry of Tryptophan Adsorbed on Gold Colloidal Nanoparticles. *J. Mol. Struct.* **2015**, *1096*, 121-128.

29. Kasture, M.; Sastry, M.; Prasad, B. L. V. Halide Ion Controlled Shape Dependent Gold Nanoparticle Synthesis with Tryptophan as Reducing Agent: Enhanced Fluorescent Properties and White Light Emission. *Chem. Phys. Lett.* **2010**, *484*, 271-275.

30. Selvakannan, P. R.; Mandal, S.; Phadtare, S.; Gole, A.; Pasricha, R.; Adyanthaya, S. D.; Sastry, M. Water-Dispersible Tryptophan-Protected Gold Nanoparticles Prepared by the Spontaneous Reduction of Aqueous Chloroaurate Ions by the Amino Acid. *J. Colloid Interface Sci.* **2004**, *269*, 97-102.

31. Palafox-Hernandez, J. P.; Tang, Z.; Hughes, Z. E.; Li, Y.; Swihart, M. T.; Prasad, P. N.; Walsh, T. R.; Knecht, M. R. Comparative Study of Materials-Binding Peptide Interactions with Gold and Silver Surfaces and Nanostructures: A Thermodynamic Basis for Biological Selectivity of Inorganic Materials. *Chem. Mater.* **2014**, *26*, 4960-4969.

32. Li, Y.; Tang, Z.; Prasad, P. N.; Knecht, M. R.; Swihart, M. T. Peptide-Mediated Synthesis of Gold Nanoparticles: Effects of Peptide Sequence and Nature of Binding on Physicochemical Properties. *Nanoscale* **2014**, *6*, 3165-3172.

33. Bhandari, R.; Knecht, M. R. Effects of the Material Structure on the Catalytic Activity of Peptide-Templated Pd Nanomaterials. *ACS Catal.* **2011**, *1*, 89-98.

34. Wunder, S.; Polzer, F.; Lu, Y.; Mei, Y.; Ballauff, M. Kinetic Analysis of Catalytic Reduction of 4-Nitrophenol by Metallic Nanoparticles Immobilized in Spherical Polyelectrolyte Brushes. *J. Phys. Chem. C* **2010**, *114*, 8814-8820.
35. Templeton, A. C.; Wuelfing, W. P.; Murray, R. W. Monolayer-Protected Cluster Molecules. *Acc. Chem. Res.* **2000**, *33*, 27-36.
36. Aryal, S.; K.C, R. B.; Bhattarai, N.; Kim, C. K.; Kim, H. Y. Study of Electrolyte Induced Aggregation of Gold Nanoparticles Capped by Amino Acids. *J. Colloid Interface Sci.* **2006**, *299*, 191-197.

FOR TABLE OF CONTENTS ONLY